Article

Synthetic Architectures of TiO/HTiO·HO, ZnO/HTiO·HO, ZnO/TiO/HTiO·HO, and ZnO/TiO Nanocomposites

Hua Gui Yang, and Hua Chun Zeng

J. Am. Chem. Soc., **2005**, 127 (1), 270-278• DOI: 10.1021/ja045253x • Publication Date (Web): 13 December 2004

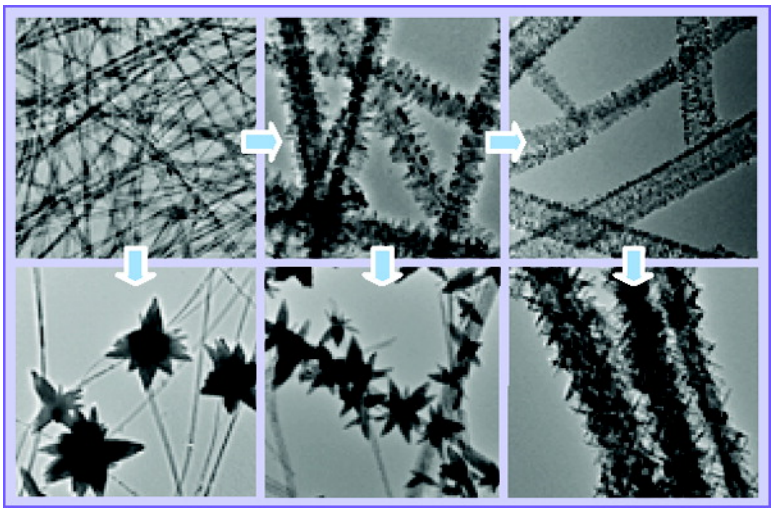

J|A|C|S
ARTICLES
Published on Web 12/13/2004

Synthetic Architectures of $TiO_2/H_2Ti_5O_{11}\cdot H_2O$, ZnO/$H_2Ti_5O_{11}\cdot H_2O$, ZnO/$TiO_2/H_2Ti_5O_{11}\cdot H_2O$, and ZnO/$TiO_2$ Nanocomposites

Hua Gui Yang and Hua Chun Zeng*

Contribution from the Department of Chemical and Biomolecular Engineering, Faculty of Engineering, National University of Singapore, 10 Kent Ridge Crescent, Singapore 119260

Received August 6, 2004; E-mail: chezhc@nus.edu.sg

Abstract: Although synthetic investigations of inorganic nanomaterials had been carried out extensively over the past decade, few of them have been devoted to fabrication of complex nanostructures that comprise multicomponents/phases (i.e., composite nanobuilding blocks), especially in the area of structural/morphological architecture. In this work, nanobelts of a protonated pentatitanate ($H_2Ti_5O_{11}\cdot H_2O$) were synthesized hydrothermally for the first time. Two technologically important transition-metal-oxides TiO_2 and ZnO were then grown respectively or sequentially onto the surface of the as-prepared nanobelts in aqueous mediums. With a main emphasis on organizational manipulation, the present investigation examines general issues of morphological complexity, synthetic interconvertibility, and material combinability related to fabrication of inorganic nanocomposites. Using this model material system, we demonstrate that complex binary and tertiary composite building blocks of $TiO_2/H_2Ti_5O_{11}\cdot H_2O$, ZnO/$H_2Ti_5O_{11}\cdot H_2O$, ZnO/$TiO_2/H_2Ti_5O_{11}\cdot H_2O$, and ZnO/$TiO_2$ can be architected stepwise in solution. Structural features of these nanocomposites have also been addressed.

Introduction

Over the past decade, fabrication of nanostructured inorganic materials has become an active research area in low dimensional materials synthesis.[1−10] However, most of the research work are focused on synthesis and morphological organizations of phase-pure nanobuilding blocks, despite an increasing interest in fabrication of nanocomposites. At present, there have been two new types of inorganic nanocomposites in addition to conventionally known "matrix-plus-a-secondary-phase" composites.[11] The first type, where two or more phases of nanoparticles are brought together by physical mixing (often with surfactant-assistance), is the most common one.[12,13] Instead of pure-phase particles, composite nanobuilding blocks have also been fabricated via various synthetic routes in recent years, showing a trend of increasing complexity for new nanocomposites.[11] In this second type of nanocomposites, nanoparticles are normally prepared into core/shell structures with spherical, beltlike, or rodlike morphologies.[14−27] Compared to type I, type II nanocomposites allow a better mixing or closer contact among

(1) Ozin, G. A. *Adv. Mater*. **1992**, *4*, 612−649.
(2) (a) Caruso, F.; Caruso, R. A.; Möhwald, H. *Science* **1998**, *282*, 1111−1114. (b) Zach, M. P.; Ng, K. H.; Penner, R. M. *Science* **2000**, *290*, 2120−2123. (c) Velikov, K. P.; Christova, C. G.; Dullens, R. P. A.; van Blaaderen, A. *Science* **2002**, *296*, 106−109. (d) Cölfen, H.; Mann, S. *Angew. Chem., Int. Ed.* **2003**, *42*, 2350−2365. (e) Park, S.; Lim, J.-H.; Chung, S.-W.; Mirkin, C. A. *Science* **2004**, *303*, 348−351.
(3) (a) Thalladi, V. R.; Whitesides, G. M. *J. Am. Chem. Soc.* **2002**, *124*, 3520−3521. (b) Kobayashi, S.; Hamasaki, N.; Suzuki, M.; Kimura, M.; Shirai, H.; Hanabusa, K. *J. Am. Chem. Soc*. **2002**, *124*, 6550−6551. (c) Smith, P. A.; Nordquist, C. D.; Jackson, T. N.; Mayer, T. S.; Martin, B. R.; Mbindyo, J.; Mallouk, T. E. *Appl. Phys. Lett.* **2000**, *77*, 1399−1401. (d) Kovtyukhova, N. I.; Mallouk, T. E. *Chem.−Eur. J.* **2002**, *8*, 4355−4363. (e) Pileni, M. P. *J. Phys. Chem. B* **2001**, *105*, 3358−3371.
(4) Sugawara, A.; Ishii, T.; Kato, T. *Angew. Chem., Int. Ed*. **2003**, *42*, 5299−5303
(5) Sampanthar, J. T.; Zeng, H. C. *J. Am. Chem. Soc*. **2002**, *124*, 6668−6675.
(6) Lou, X. W.; Zeng, H. C. *J. Am. Chem. Soc.* **2003**, *125*, 2697−2704.
(7) Krumeich, F.; Muhr, H.-J.; Niederberger, M.; Bieri, F.; Schnyder, B.; Nesper, R. *J. Am. Chem. Soc.* **1999**, *121*, 8324−8331.
(8) Ying, J. Y.; Mehnert, C. P.; Wong, M. S. *Angew. Chem., Int. Ed*. **1999**, *38*, 56−77.
(9) Thomas, J. M. *Angew. Chem., Int. Ed*. **1999**, *38*, 3588−3628.
(10) Spahr, M. E.; Bitterli, P.; Nesper, R.; Müller, M.; Krumeich, F.; Nissen, H.-U. *Angew. Chem., Int. Ed.* **1998**, *37*, 1263−1265.
(11) (a) van Bommel, K. J. C.; Friggeri, A.; Shinkai, S. *Angew. Chem., Int. Ed*. **2003**, *42*, 980−999. (b) Zeng, H. C. *Handbook of Organic−Inorganic Hybrid Materials and Nanocomposites*; Nanocomposites. American Scientific Publishers: New York, 2003; Vol. 2, Chapter 4, pp 151−180.
(12) Zeng, H.; Li, J.; Liu, J. P.; Wang, Z. L.; Sun, S. *Nature* **2002**, *420*, 395−398.
(13) Redl, F. X.; Cho, K.-S.; Murray, C. B.; O'Brien, S. *Nature* **2003**, *423*, 968−971.
(14) Hong, B. H.; Bae, S. C.; Lee, C.-W.; Jeong, S.; Kim, K. S. *Science* **2001**, *294*, 348−351.
(15) Lauhon, L. J.; Gudiksen, M. S.; Wang, D.; Lieber, C. M. *Nature* **2002**, *420*, 57−61.
(16) Sloan, J.; Terrones, M.; Nufer, S.; Friedrichs, S.; Bailey, S. R.; Woo, H.-G.; Rühle, M.; Hutchison, J. L.; Green, M. L. H. *J. Am. Chem. Soc*. **2002**, *124*, 2116−2117.
(17) Wilson, M. *Nano Lett.* **2004**, *4*, 299−302.
(18) Wu, Y.; Fan, R.; Yang, P. *Nano Lett.* **2002**, *2*, 83−86.
(19) He, R.; Law, M.; Fan, R.; Kim, F.; Yang, P. *Nano Lett.* **2002**, *2*, 1109−1112.
(20) Gudiksen, M. S.; Lauhon, L. J.; Wang, J.; Smith, D. C.; Lieber, C. M. *Nature* **2002**, *415*, 617−620.
(21) Pyun, J.; Matyjaszewski, K. *Chem. Mater*. **2001**, *13*, 3436−3448.
(22) Urbach, A. R.; Love, J. C.; Prentiss, M. G.; Whitesides, G. M. *J. Am. Chem. Soc.* **2003**, *125*, 12704−12705.
(23) Mokari, T.; Rothenberg, E.; Popov, I.; Costi, R.; Banin, U. *Science* **2004**, *304*, 1787−1790.
(24) Wu, D.; Ge, X.; Zhang, Z.; Wang, M.; Zhang, S. *Langmuir* **2004**, *20*, 5192−5195.
(25) Danek, M.; Jensen, K. F.; Murray, C. B.; Bawendi, M. G. *Chem. Mater*. **1996**, *8*, 173−180.
(26) Manna, L.; Scher, E. C.; Li, L.-S.; Alivisatos, A. P. *J. Am. Chem. Soc.* **2002**, *124*, 7136−7145.
(27) Hwang, J.; Min, B.; Lee, J. S.; Keem, K.; Cho, K.; Sung, M.-Y.; Lee, M.-S.; Kim, S. *Adv. Mater*. **2004**, *16*, 422−425.

10.1021/ja045253x CCC: $30.25

the different phases. In a broader sense, inorganic nanostructures to which a metallic seed or a liquid droplet (metallic catalysts) is attached can also be classified into this type.[28] It should be mentioned that in most of the investigations for type II nanocomposites the research has been limited to chemical modification when a secondary phase is introduced.[14−27] Morphological and organizational control, however, remains largely an unattained research subject despite nanomaterials having been utilized as substrates or templates.[6,29,30]

To fabricate composite nanobuilding blocks, structural and geometrical architectures among various nanocomponents should be further addressed. Apart from alternation of electronic states by creating interfacial regions (such as $p-n$ junctions),[18,20] the organization pattern and shape of each component in an integrated nanocomposite further determine its ultimate physicochemical properties and thus performance.[31−33] For example, chemical reactivity, mass diffusivity, and electrooptic activity, etc. are closely related to crystallographic orientation and morphological arrangement of nanocomponents within a composite. Furthermore, intrinsic chemical reactivity and lattice compatibility among the various nanocomponents should also be investigated.[34] Due to different process conditions, for instance, some of existing phases may dissolve or convert into other phases during the subsequent addition of new phases. Once this occurs, synthetic complexity of nanocomposites will be increased, and selection of compatible processing routes would then become an important prerequisite for the precise nanocomponent integration, especially when a total wet synthetic strategy is the aim.

To address the above fundamental issues in designing new nanocomposites, this contribution explores the synthetic architectures of a range of metal-oxide nanocomposites under wet conditions. Material combination of two technologically important metal oxides, TiO_2 and ZnO,[34−46] is investigated in this work, together with their depositions on a degradable protonated pentatitanate (i.e., $H_2Ti_5O_{11}\cdot H_2O$) nanobelt substrate; note that there are also many important applications of the layered titanates.[47−57] With a main emphasis on architectural manipulation, the present work, as part of our continuous effort in fabricating complex inorganic nanostructured building blocks,[6,30] is directed to an exploitation of structural complexity, synthetic convertibility, and material combinability of binary and tertiary nanocomposites of $TiO_2/H_2Ti_5O_{11}\cdot H_2O$, $ZnO/H_2Ti_5O_{11}\cdot H_2O$, $ZnO/TiO_2/H_2Ti_5O_{11}\cdot H_2O$, and ZnO/TiO_2 with a step-by-step processing technique in aqueous reaction mediums.

Experimental Section

Materials Preparation. Hydrochloric acid (HCl, 1.5 M) was used to adjust the pH of deionized water (1.0 L) to 2. Titanium tetrafluoride (TiF_4, Aldrich Chemical) was then dissolved in this solution to give a concentration of 0.040 M, during which pH was changed to 1.8. The TiF_4 solution is clear and stable under room temperature, and deionized water was used to adjust the concentration for further use. The concentration of TiF_4 adopted herein was low to ensure a slow hydrolysis rate. In principle, $TiCl_4$ would also produce similar results, but it would be less manageable, owing to its fast hydrolysis rate. Four major synthetic steps were designed in the present materials preparation. In the first step, protonated pentatitanate ($H_2Ti_5O_{11}\cdot H_2O$) nanobelts were synthesized by a novel alkali hydrothermal process developed in this work. The process involved keeping 30 mL of as-prepared 0.040 M TiF_4 aqueous solution containing 10 g of NaOH in a Teflon-lined stainless autoclave under 180 °C for 48−50 h and then washing the white gel-like product with a 0.50 M HCl solution and deionized water thoroughly. In the second step, 0.01 g of white product from step 1 was put into 40 mL of a diluted TiF_4 solution (typically at 0.008 M) maintained at 50 °C for a desired period of time to prepare $TiO_2/H_2Ti_5O_{11}\cdot H_2O$ nanocomposites. After the reactions, the composite samples were washed with deionized water and dried in a vacuum at room temperature. In the third step, pure anatase TiO_2 nanorods composed of orderly arranged uniform nanocrystallites were fabricated just by hydrothermally treating $TiO_2/H_2Ti_5O_{11}\cdot H_2O$ (which was produced from the step 2) in 30 mL of deionized water under 120 °C for 21 h. The product from this step was also washed with deionized water and dried in a vacuum at room temperature. In the final step, $ZnO/H_2Ti_5O_{11}\cdot H_2O$ or ZnO/TiO_2 nanocomposites were generated with an aqueous reaction method. Typically, a 0.010 M zinc sulfate ($ZnSO_4$) aqueous solution containing ammonium fluoride (NH_4F, used as a complexing agent; molar ratio of $NH_4^+/Zn^{2+} = 30$) was prepared first, and the pH value was adjusted to 11.66 with a NaOH solution (5 M). Then, 0.005−0.015 g of the final product prepared from the step 1 or step 3 was added into 40 mL of the above as-prepared $ZnSO_4$ solution maintained at 60 °C for 7−15 h. The generated $ZnO/H_2Ti_5O_{11}\cdot H_2O$ or ZnO/TiO_2 nanocomposites were also washed thoroughly with deionized water and dried in a vacuum at room temperature.

Materials Characterization. Crystallographic phases of the prepared nanostructures from each major synthetic step were investigated by an X-ray diffraction method (XRD; Shimadzu XRD-6000, Cu Kα radiation). The dimension, morphology, and chemical composition of the samples were examined using scanning electron microscopy and energy-dispersive X-ray spectroscopy (SEM/EDX; JSM-5600LV), transmission electron microscopy (TEM; JEM 2010, 200 kV), selected area electron diffraction (SAED), and high-resolution transmission electron micros-

(28) Barrelet, C. J.; Wu, Y.; Bell, D. C.; Lieber, C. M. *J. Am. Chem. Soc.* **2003**, *125*, 11498−11499.
(29) Wei, X. M.; Zeng, H. C. *J. Phys. Chem. B* **2003**, *107*, 2619−2622.
(30) Liu, B.; Zeng, H. C. *J. Phys. Chem. B* **2004**, *108*, 5867−5874.
(31) Bell, A. T. *Science* **2003**, *299*, 1688−1691.
(32) Valden, M.; Lai, X.; Goodman, D. W. *Science* **1998**, *281*, 1647−1650.
(33) Zeng, H. C. In *The Dekker Encyclopedia of Nanoscience and Nanotechnology*; Marcel Dekker: New York, 2004; pp 2539−2550.
(34) Yang, H. G.; Zeng, H. C. *J. Phys. Chem. B* **2004**, *108*, 819−823.
(35) Yang, H. G.; Zeng, H. C. *Angew. Chem., Int. Ed.* **2004**, *43*, 5026−5029.
(36) Huang, M. H.; Mao, S.; Feick, H.; Yan, H.; Wu, Y.; Kind, H.; Weber, E.; Russo, R.; Yang, P. *Science* **2001**, *292*, 1897−1899.
(37) Liu, B.; Zeng, H. C. *J. Am. Chem. Soc.* **2003**, *125*, 4430−4431.
(38) Greene, L. E.; Law. M.; Goldberger, J.; Kim, F.; Johnson, J. C.; Zhang, Y.; Saykally, R. J.; Yang, P. *Angew. Chem., Int. Ed.* **2003**, *42*, 3031−3034.
(39) Pacholski, C.; Kornowski, A.; Weller, H. *Angew. Chem., Int. Ed.* **2002**, *41*, 1188−1191.
(40) Gao, P. X.; Ding, Y.; Wang, Z. L. *Nano Lett.* **2003**, *3*, 1315−1320.
(41) Lao, J. Y.; Wen, J. G.; Ren, Z. F. *Nano Lett.* **2002**, *2*, 1287−1291.
(42) Huang, M. H.; Wu, Y.; Feick, H.; Tran, N.; Weber, E.; Yang, P. *Adv. Mater.* **2001**, *13*, 113−116.
(43) Yan, H.; He, R.; Pham, J.; Yang, P. *Adv. Mater.* **2003**, *15*, 402−405.
(44) Vayssiers, L. *Adv. Mater.* **2003**, *15*, 464−466.
(45) Guo, L.; Ji, Y. L.; Xu, H.; Simon, P.; Wu, Z. *J. Am. Chem. Soc.* **2002**, *124*, 14864−14865.
(46) Yamabi, S.; Imai, H. *J. Mater. Chem.* **2002**, *12*, 3773−3778.
(47) Chen, Q.; Zhou, W.; Du, G.; Peng, L. *Adv. Mater.* **2002**, *14*, 1208−1211.
(48) Sasaki, T.; Komatsu, Y.; Fujiki, Y. *Chem. Mater.* **1992**, *4*, 894−899.
(49) Izawa, H.; Kikkawa, S.; Koizumi, M. *J. Phys. Chem. B* **1982**, *86*, 5023−5026.
(50) Zhu, Y.; Li, H.; Koltypin, Y.; Hacohen, Y. R.; Gedanken, A. *Chem. Commun.* **2001**, 2616−2617.
(51) Yin, S.; Uchida, S.; Fujishiro, Y.; Aki, M.; Sato, T. *J. Mater. Chem.* **1999**, *9*, 1191−1196.
(52) (a) Sasaki, T.; Watanabe, M.; Fujiki, Y.; Kitami, Y. *Chem. Mater.* **1994**, *6*, 1749−1756. (b) Sasaki, T.; Izumi, F.; Watanabe, M. *Chem. Mater.* **1996**, *8*, 777−782.
(53) Sasaki, T.; Watanabe, M.; Komatsu, Y.; Fujiki, Y. *Inorg. Chem.* **1985**, *24*, 2265−2271.
(54) (a) Tian, Z. R.; Voigt, J. A.; Liu, J.; Mckenzie, B.; Xu, H. *J. Am. Chem. Soc.* **2003**, *125*, 12384−12385. (b) Sun, X.; Li, Y. *Chem.−Eur. J.* **2003**, *9*, 2229−2238. (c) Zhu, H.; Gao, X.; Lan, Y.; Song, D.; Xi, Y.; Zhao, J. *J. Am. Chem. Soc.* **2004**, *126*, 8380−8381.
(55) Le Bail, A.; Fourquet, J. L. *Mater. Res. Bull.* **1992**, *27*, 75−85.
(56) Cheng, S.; Wang, T. *Inorg. Chem.* **1989**, *28*, 1283−1289.
(57) Anderson, M. W.; Klinowski, J. *Inorg. Chem.* **1990**, *29*, 3260−3263.

copy with EDX (HRTEM/EDX; JEM 3010, 300 kV). Thermogravimetric analysis (TGA/DTG; Shimadzu TGA-50) was also performed to determine the metal oxide content in the as-prepared $H_2Ti_5O_{11}\cdot H_2O$. The TGA/DTG measurements were carried out at a heating rate of 10 °C min^{-1} in a pure nitrogen atmosphere (50 mL min^{-1}).[58−60]

Results and Discussion

Preparation of $H_2Ti_5O_{11}\cdot H_2O$ Nanobelts. As a starting structural basis, protonated pentatitanate $H_2Ti_5O_{11}\cdot H_2O$ nanobelts were synthesized for the first time in this work. Figure 1 shows three TEM images of the prepared $H_2Ti_5O_{11}\cdot H_2O$ nanobelts (the first step, Experimental Section). The nanobelts are flexible and can be well-dispersed (Figure 1A). With the selection of synthetic parameters (e.g., concentration), the size of the nanobelts can be further controlled (see SI-1). The $H_2Ti_5O_{11}\cdot H_2O$ nanobelts are single-crystalline and have a rectangular morphology owing to intrinsic structural anisotropy and growth rate (r_{hkl}) variation in all three principal directions $r_{001} > r_{100} > r_{010}$. The HRTEM image recorded perpendicularly to the nanobelt (i.e., along [010] direction) clearly shows that the nanobelt has a layered structure with interplanar distances of $d_{200} = 0.83$ nm and $d_{004} = 0.31$ nm. In excellent agreement with the literature value,[61] the interplanar angle between the ⟨100⟩ and ⟨001⟩ shown in Figure 1C is ca. 124°. The XRD investigation on these nanobelts is shown in Figure 2A. All the peaks correspond well to the $H_2Ti_5O_{11}\cdot H_2O$ phase; our calculated lattice constants are indeed identical to a monoclinic unit cell that has $a = 2.0005$ nm, $b = 0.3763$ nm, $c = 1.4998$ nm, and $\beta = 124.01°$ (i.e., $d_{200} = 0.829$ nm, $d_{020} = 0.1882$ nm, and $d_{004} = 0.3111$ nm).[61] Figure 3 illustrates an idealized structural representation of the protonated pentatitanate $H_2Ti_5O_{11}\cdot H_2O$ in projection along the [010] and [001] directions. This compound is composed of corrugated strips of edge-sharing TiO_6 octahedra. Each strip is five-octahedron wide, and the strips further corner-join to form stepped sheets. The unit cells (enclosed by dotted lines) belong to the *C*-base-centered monoclinic symmetry (space group of $H_2Ti_5O_{11}\cdot H_2O$: $C2/m$, $Z = 4$); open circles denote H_2O (or H_3O^+) at $y = 0$ and $^1/_2$, respectively. In such a structure, water molecules may be arranged in a single row in an interlayer space because of a smaller interlayer distance (0.83 nm), in analogue to that of the fully hydrated phase $H_2Ti_5O_{11}\cdot 3H_2O$ (1.042 nm).[48] The monohydrous phase is relatively stable and it will not change to some swelled phase even in the environment with abundant water. This solid compound, however, is unstable under the irradiation of a focused electron beam. The SAED pattern in Figure 1B shows some displacement of original monoclinic *h*0*l* spots, indicating that a structural conversion has taken place for the area (circled) with the electron beam exposure (SI-2). In certain cases, indeed, the anatase TiO_2 pattern (e.g., [010] zone spots) can be clearly observed for the decomposing nanobelts (see SI-3 and Figure 9). On the basis of the orientation of anatase diffraction pattern, it is known that this reconstructing process requires only a minimal structural alternation of TiO_6 octahedra after removal of intercalated water, as depicted in Figure 3C.

To confirm chemical composition of the $H_2Ti_5O_{11}\cdot H_2O$ nanobelts, TGA investigation has been further carried out; Figure 4 indicates a total weight loss of 9.89% over the temperature range of 27.5−600 °C. The theoretical value of weight loss of $H_2Ti_5O_{11}\cdot H_2O$ during the dehydration reaction (to TiO_2) is 8.28%. The small difference between the experimental and theoretical values may be simply due to loss of water molecules physically adsorbed on the surface or trapped in the interparticle space. However, it has also been assumed that free interlayer

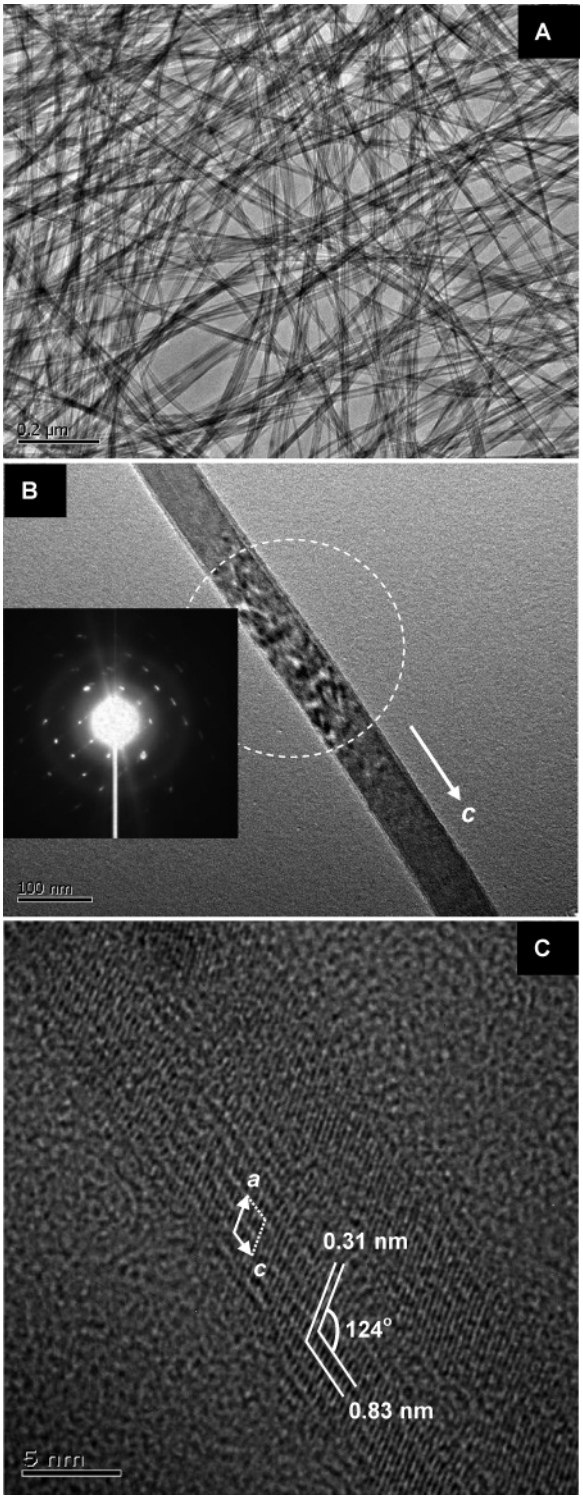

Figure 1. (A) TEM image of synthesized $H_2Ti_5O_{11}\cdot H_2O$ nanobelts at 180 °C for 50 h (see Experimental Section for details), (B) SAED pattern of a free-standing $H_2Ti_5O_{11}\cdot H_2O$ nanobelt (recorded along *b*-axis for the circled area), and (C) HRTEM image of a $H_2Ti_5O_{11}\cdot H_2O$ nanobelt.

(58) Ji, L.; Lin, J.; Zeng, H. C. *J. Phys. Chem. B* **2000**, *104*, 1783−1790.
(59) Xu, Z. P.; Zeng, H. C. *Chem. Mater.* **2001**, *13*, 4564−4572.
(60) Lou, X. W.; Zeng, H. C. *Chem. Mater.* **2002**, *14*, 4781−4789.
(61) Joint Committee on Powder Diffraction Standards, International Centre for Diffraction Data, Card Nos. 44-0130 and 44-0131, Swarthmore, PA, 1996.

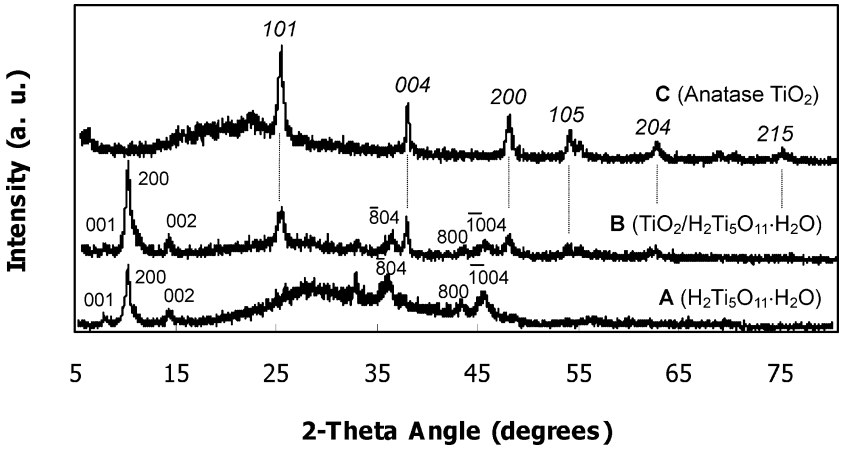

Figure 2. XRD patterns showing materials that were involved at different stages: (A) $H_2Ti_5O_{11}\cdot H_2O$ nanowires (Figure 1A). (B) $TiO_2/H_2Ti_5O_{11}\cdot H_2O$ nanocomposite (Figure 5) prepared in 0.008 M TiF_4 aqueous solution (50 °C, 20 h) by using $H_2Ti_5O_{11}\cdot H_2O$ nanowires shown in Figure 1A as substrate. (C) TiO_2 nanorods (Figure 6) derived from $TiO_2/H_2Ti_5O_{11}\cdot H_2O$ nanocomposite under hydrothermal conditions (120 °C, 21 h). Anatase phase (in B and C) is indexed with italic numbers. The humps in the background are due to the glass sample holder used in the measurement.

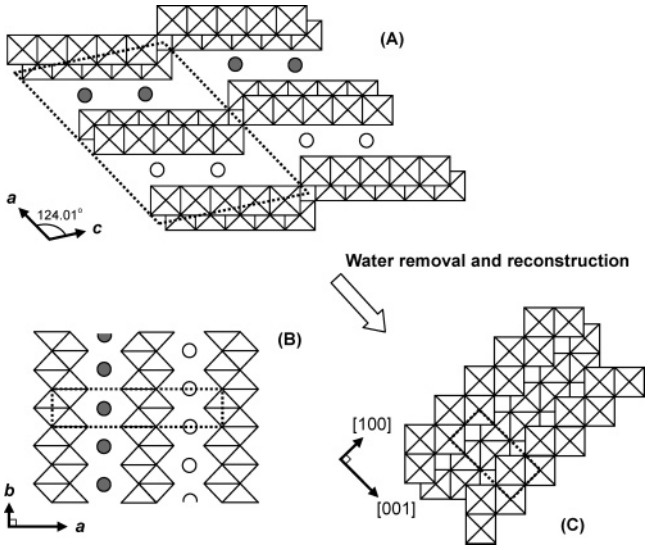

Figure 3. Schematic representations of crystal structure for the layered $H_2Ti_5O_{11}\cdot H_2O$ (A and B) and its reconstruction to anatase TiO_2 (C; the tetragonal unit cell is indicated with dotted lines) after water removal. TiO_6 octahedra are represented by squares in parts A and C and twinned triangles in part B. Water molecules are indicated with open and filled circles (y = 0 and $^1/_2$, respectively). The unit cells (A and B; enclosed by dotted lines) are *C*-base centered monoclinic for $H_2Ti_5O_{11}\cdot H_2O$, where part A is projected along [010] direction, while part B, along [001].

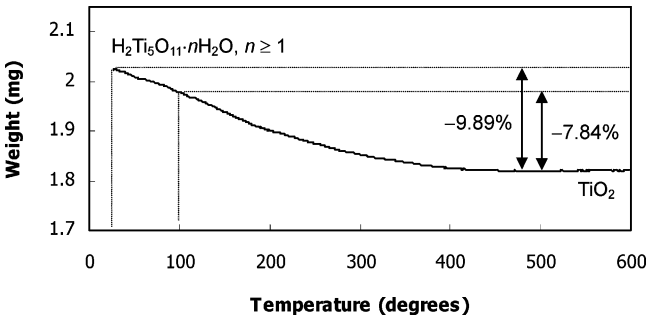

Figure 4. TGA scan for the $H_2Ti_5O_{11}\cdot H_2O$ nanobelts with a heating rate of 10 °C min^{-1} in a nitrogen atmosphere (flow rate at 50 mL min^{-1}).

water of $H_2Ti_5O_{11}\cdot 3H_2O$ could be evaporated up to 100 °C forming the stable $H_2Ti_5O_{11}\cdot H_2O$ (i.e., $H_2Ti_5O_{11}\cdot H_2O$ does not decompose at 100 °C).[48] In such a case, the weight loss is then to be 7.84% over 100−600 °C for our sample (Figure 4), which has a smaller difference compared to the theoretical value (vs 8.28%). In fact, our data are very close to the reported values in the literature (7.5−7.7% over 100−500 °C).[48] The formation mechanism of our as-prepared $H_2Ti_5O_{11}\cdot H_2O$ nanobelts could be further elucidated. First, sodium pentatitanate ($Na_2Ti_5O_{11}\cdot H_2O$) nanobelts were formed under concentrated NaOH solution. The formed $Na_2Ti_5O_{11}\cdot H_2O$ could then be protonated while preserving their pristine layered structures. Consistent with the cation-exchange mechanism,[47] our EDX study indeed shows only Ti and O are present (note that H is not detectable with EDX) in the prepared $H_2Ti_5O_{11}\cdot H_2O$ nanobelts, free of inclusion of Na cations.

Preparation of $TiO_2/H_2Ti_5O_{11}\cdot H_2O$ Nanocomposites. Due to its special crystal structure (Figure 3), the protonated pentatitanate nanobelts could be used as a template to form nanocomposites $TiO_2/H_2Ti_5O_{11}\cdot H_2O$ where TiO_2 crystallites are deposited into short-nanorod arrays. In Figure 5, dilute aqueous TiF_4 solution (0.008 M) was used to grow anatase TiO_2 on the protonated pentatitanate nanobelts at 50 °C. When the time of reaction is short (e.g., 3 h), the deposited nanorods (diameter and length: 10 and 70 nm) that are perpendicular to the propagating axis (*c*-axis) of the nanobelts were well aligned. If the time is extended to 20 h, the aligned TiO_2 nanorods would become much bigger (diameter and length: 20 and 100 nm). During the TiO_2 deposition, the original structure of the protonated pentatitanate nanobelts is well preserved, which is confirmed in the related XRD patterns (Figure 2B), noting that all major diffraction peaks can be observed for both solid phases. The representative SAED pattern shown in Figure 5D is essentially similar to that of Figure 6D; a detailed analysis of these diffraction patterns will be presented in Figure 6D shortly. This ED analysis, together with HETEM investigation (lattice fringe of d_{200} = 0.19 nm can be observed; SI-3), indicates that the individual TiO_2 nanorod branches are largely single-crystalline and their growth directions are along ⟨001⟩. The anatase TiO_2 polymorph belongs to the tetragonal symmetry with lattice constants a = 0.378 52 nm and c = 0.951 39 nm (SG: $I4_1/amd$).[62] In our $TiO_2/H_2Ti_5O_{11}\cdot H_2O$ nanocomposites,

(62) Joint Committee on Powder Diffraction Standards, International Centre for Diffraction Data, Card No. 21-1272, Swarthmore, PA, 1996.

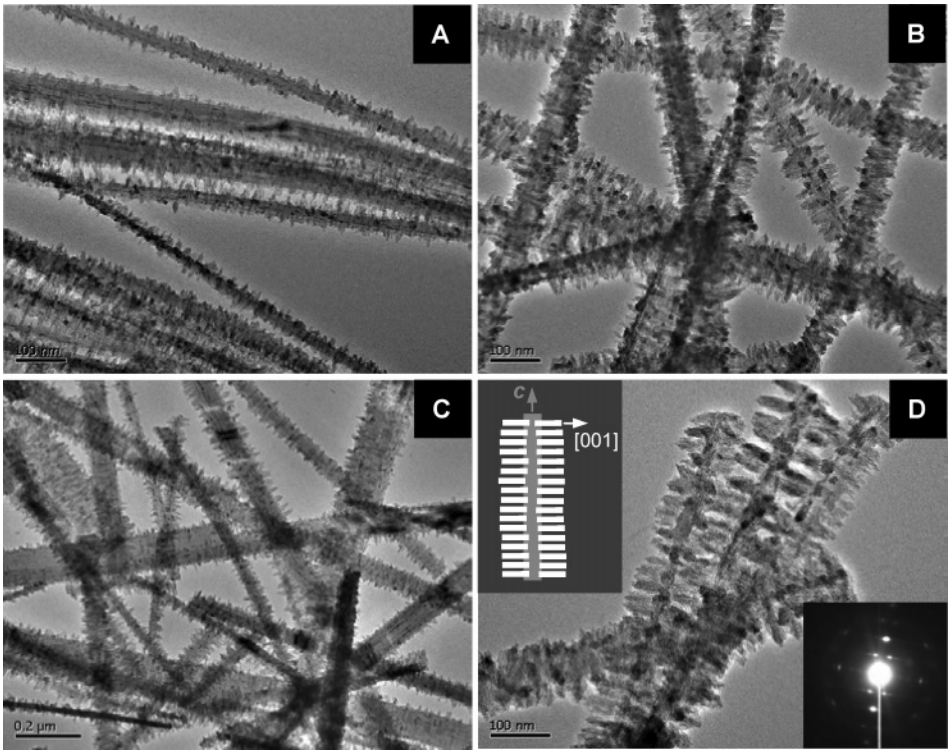

Figure 5. TEM images of $TiO_2/H_2Ti_5O_{11}\cdot H_2O$ nanocomposites prepared in 40 mL of 0.008 M TiF_4 aqueous solution at 50 °C for different reaction times (A and B) 3 h, (C) 6 h, and (D) 20 h. Insets in part D indicate orientations of the two different types of nanocrystals (TiO_2 in white) and a typical SAED pattern recorded for a free-standing nanocomposite rod.

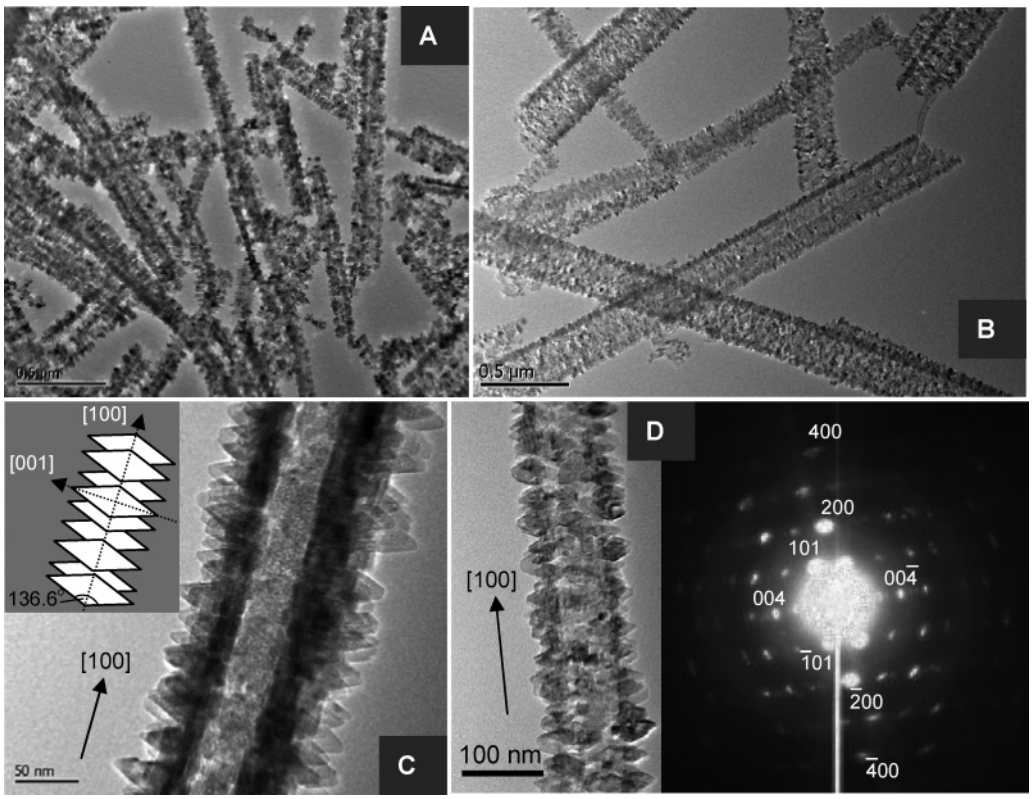

Figure 6. One-dimensional anatase TiO_2 nanocrystal arrays derived from $TiO_2/H_2Ti_5O_{11}\cdot H_2O$ nanocomposites (of Figure 5) under hydrothermal treatments (120 °C, 15−21 h): (A and B) overall product morphologies, (C and D) detailed images, and an SAED pattern for bipyramidal TiO_2 nanocrystals (building blocks; inset of part C) which are bounded with eight {101} planes.

on the other hand, the {010} planes of anatase TiO_2 nanorod arrays are parallel to the {010} planes of $H_2Ti_5O_{11}\cdot H_2O$ substrate. Considering the large lattice mismatches between the two interfacial planes, it is believed that the edge-sharing TiO_6 octahedra on the side walls of the $H_2Ti_5O_{11}\cdot H_2O$ nanobelt must have undergone a rearrangement (Figure 3C) during TiO_2

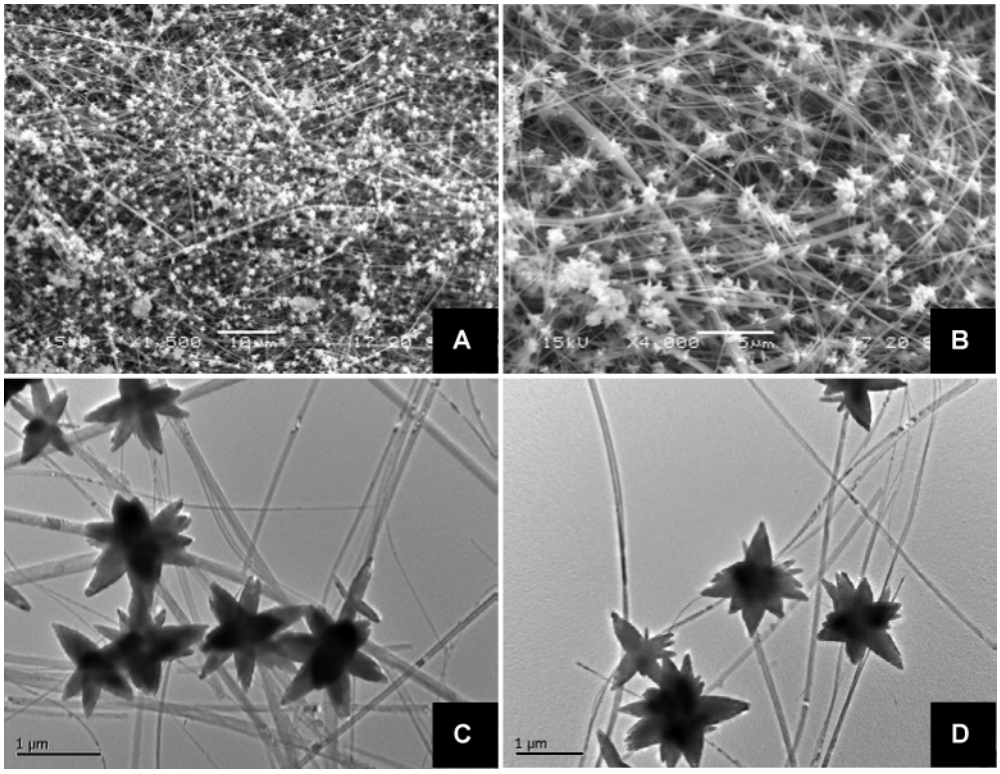

Figure 7. SEM images (A and B) and TEM images (C and D) of the flowerlike $ZnO/H_2Ti_5O_{11}\cdot H_2O$ nanocomposite prepared by adding as-prepared $H_2Ti_5O_{11}\cdot H_2O$ nanobelts (Figure 1) into a 0.010 M $ZnSO_4$ aqueous solution containing ammonium fluoride (molar ratio $NH_4^+/Zn^{2+} = 30$, pH = 11.66) at 60 °C for 7 h.

nanorod deposition at 50 °C. The direct deposition process relies on in situ nuclear formation and subsequent oriented crystal growth of anatase on $H_2Ti_5O_{11}\cdot H_2O$ nanobelts. The degree of supersaturation of titanium source in our experiments was low to maintain a slow deposition rate of TiO_2.[63,64] One important observation here is hardening of the $H_2Ti_5O_{11}\cdot H_2O$ nanobelts when the anatase TiO_2 was deposited. In general, straighter and shorter composite products can be attained after the deposition reactions.

The above-prepared $TiO_2/H_2Ti_5O_{11}\cdot H_2O$ nanocomposites could be further converted into phase-pure anatase TiO_2 nanocrystal arrays with additional hydrothermal treatments (e.g., at 120 °C), as exampled in Figure 6. These one-dimensional nanostructures are composed of smaller primary TiO_2 nanocrystals (width and length: about 20 and 70 nm) which are bounded with eight {101} planes. The nanocrystals are aligned with each other along ⟨100⟩ and ⟨001⟩ directions respectively, as revealed by the interplanar angles among the eight crystal planes of TiO_2 bipyramids (e.g., 136.6°, Figure 6C), which is further confirmed in our SAED investigation. The [010] zone diffraction spots of the tetragonal phase are fairly focused, indicating an excellent alignment among the individual crystals along both ⟨100⟩ and ⟨001⟩ directions, and a pseudo-single-crystal nature for the overall TiO_2 nanocrystal arrays. In this agreement, our HRTEM investigation on the individual TiO_2 nanocrystals also shows that the {100} crystal planes (i.e., lattice fringes of $d_{200} = 0.19$ nm, SI-4)[62] of the anatase phase are perpendicular to the propagating direction of the TiO_2 arrays. Our XRD result (Figure 2C) further confirms that the TiO_2 arrays are indeed phase-pure anatase. Depending on the process parameters adopted, these arrays can be extended to as long as a few micrometers in length and a few hundred nanometers in breadth (Figure 6A and 6B). Interestingly, Figure 6C reveals the existence of hollow interiors (channel-like; the image contrast between the dark edge and pale center) along the crystal arrays due to the dissolution of $H_2Ti_5O_{11}\cdot H_2O$ nanobelts during the hydrothermal treatment. In this regard, the TiO_2 previously grown on the protonated pentatitanate nanobelts (i.e., those in Figure 5) may also act as a template to facilitate this phase conversion, as evidenced in the orientation conservation of the TiO_2 nanostructures.

Preparation of $ZnO/H_2Ti_5O_{11}\cdot H_2O$ Nanocomposites. The as-prepared protonated pentatitanate nanobelts can also be used as substrates to synthesize $ZnO/H_2Ti_5O_{11}\cdot H_2O$ nanocomposites. Figure 7 shows SEM/TEM images of some flowerlike composite products at different magnifications. The deposited ZnO "flowers" on $H_2Ti_5O_{11}\cdot H_2O$ nanobelts ("stems") usually have multiple pods with a diameter of ~100−200 nm and a length of 500−800 nm. Chemical composition (such as Zn, Ti, and O) of the $ZnO/H_2Ti_5O_{11}\cdot H_2O$ was further confirmed with the EDX method, and the XRD pattern in Figure 8A clearly shows the copresence of diffraction peaks of ZnO (in wurtzite phase)[65] and $H_2Ti_5O_{11}\cdot H_2O$.

In the ramose ZnO nanostructure, there is a central pod (i.e., the dark hexagon in Figure 9A) grown perpendicularly to the {010} planes of the nanobelt support, i.e., [0001] and [11−20] axes of ZnO are parallel to *b*- and *c*-axes of $H_2Ti_5O_{11}\cdot H_2O$, respectively. The multiple pods are then extended normally to

(63) Yang, H. G.; Zeng, H. C. *Chem. Mater.* **2003**, *15*, 3113−3120.
(64) Yang, H. G.; Zeng, H. C. *J. Phys. Chem. B* **2003**, *107*, 12244−12256.
(65) Joint Committee on Powder Diffraction Standards, International Centre for Diffraction Data, Card No. 36-1451, Swarthmore, PA, 1996.

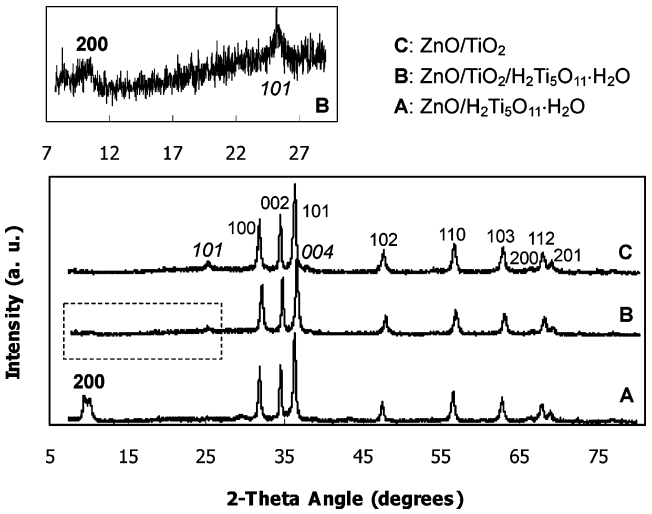

Figure 8. XRD patterns for different ZnO-containing nanocomposites: (A) $ZnO/H_2Ti_5O_{11}\cdot H_2O$ (Figure 7), (B) $ZnO/TiO_2/H_2Ti_5O_{11}\cdot H_2O$ (Figure 10), and (C) ZnO/TiO_2 (Figure 11). Anatase phase (in parts B and C) is indexed with italic numbers, $H_2Ti_5O_{11}\cdot H_2O$, in bold (in parts A and B), and ZnO, in smaller numbers. The framed area in the pattern B is detailed in the upper box.

the six prismatic side planes of the central ZnO, each having [0001] as its own growing axis, noting that the preferred [0001] has been observed on many metal oxide supports regardless of lattice compatibility. In Figure 9B, the crystallographic relationships among the ZnO pods and $H_2Ti_5O_{11}\cdot H_2O$ template is further demonstrated. The SAED result shows a superimposition of two different sets of diffraction patterns. The first set of diffraction spots belongs to the [1−100] zone of wurtzite ZnO, and the orientation of spot pattern indicates that the ZnO pod perpendicular to the nanobelt edge is indeed growing along [0001]. On the other hand, as discussed in Figure 1, the monoclinic $H_2Ti_5O_{11}\cdot H_2O$ stem is decomposing into the tetragonal TiO_2 under the irradiation of a TEM electron beam, which is reflected in the detection of [010] zone spots of the anatase phase. The HRTEM image in Figure 9C shows that the wurtzite ZnO synthesized is highly single-crystalline (lattice fringes $d_{10-11} = 0.25$ nm). In contrast, the decomposing $H_2Ti_5O_{11}\cdot H_2O$ is rather disordered (Figure 9D). Consistent with our SAED result, however, the d_{200}, d_{002}, and d_{101} lattice fringes of the anatase TiO_2 can be observed clearly in this HRTEM image.

Preparation of $ZnO/TiO_2/H_2Ti_5O_{11}\cdot H_2O$ Nanocomposites. In addition to the formation of $ZnO/H_2Ti_5O_{11}\cdot H_2O$, ZnO can also be deposited onto the $TiO_2/H_2Ti_5O_{11}\cdot H_2O$ composite template prepared earlier (Figure 5), resulting in an even more complex nanocomposite $ZnO/TiO_2/H_2Ti_5O_{11}\cdot H_2O$. Compared to the previous case in Figure 7, less branching of ZnO is observed in this material combination; the short ZnO nanopods appear mostly as "leaves" (instead of "flowers") on the bamboolike nanostructures. In addition to the [0001] standing ZnO monopods (Figure 10C), bipods, and tripods (Figure 10D and 10E), other types of branching have also been observed. Among the ZnO multipods displayed in Figure 10F−H, for example, a common angle between the ZnO "leaves" and $TiO_2/H_2Ti_5O_{11}\cdot H_2O$ "stems" is observed at ca. 50°, which reflects a certain interfacial crystallographic relationship between the ZnO and $TiO_2/H_2Ti_5O_{11}\cdot H_2O$ that will be discussed shortly in the next subsection. The coexistence of the three solid phases in this composite has also been confirmed in our XRD investigation reported in Figure 8B.

Preparation of ZnO/TiO_2 Nanocomposites. Using the one-dimensional TiO_2 nanostructured arrays (Figure 6) as a core phase, ordered ZnO nanorod arrays could be organized as a surface phase. Figure 11 shows the TEM images of a ZnO/TiO_2 nanocomposite where ZnO nanorods (diameter at ca. 80 nm) were formed on the TiO_2 support with a specific acute angle of 50° between the propagating axis of ZnO nanorods and the axial direction of overall nanostructures (i.e., the [100] direction of TiO_2, Figure 11C). As illustrated in Figure 12, the axial direction of the interior TiO_2 nanostructures is along ⟨100⟩ and the TiO_2 bipyramidal units are single-crystalline with the ⟨001⟩ directions along its axis. It could be concluded that the ZnO prefers to nucleate on the {103} crystal steps on the surface of the bipyramidal TiO_2. Furthermore, it is known that the lattice mismatch between the {103} planes of anatase TiO_2 and the {0002} planes of wurtzite ZnO is very small, noting that the interplanar distances of d_{103} (0.2431 nm, TiO_2) and d_{0002} (0.2605 nm, ZnO) is rather similar, which might promote a continued heteroepitaxial growth.[62,65] A detailed investigation on interfacial structure is currently in progress. An HRTEM image of the ZnO nanorods shown in Figure 10C indicates excellent crystallinity of the prepared ZnO nanorods, and the XRD pattern of Figure 8C also shows that the final product indeed consists of both wurtzite ZnO and anatase TiO_2.

General Structural Features and Their Implications. On the basis of the above syntheses, several structural properties can be engineered for this family of nanocomposites. For example, dimension, flexibility, and/or rigidness of the resultant nanocomposites have now been known to be dependent strongly on the reaction conditions and the primary phase chosen. Among all these properties, one common structural feature that all the above nanocomposites possess is their "hairy" surface phases. Instead of normal planarized secondary phase coatings, the presence of extruding external phases would lead to the following property implications:

(i) In $TiO_2/H_2Ti_5O_{11}\cdot H_2O$, the fishbonelike TiO_2 superstructures formed on the top of $H_2Ti_5O_{11}\cdot H_2O$ nanobelts offer a number of self-organization possibilities among the composite nanobuilding blocks. For example, parallel (Figure 5A and 5D) and netted (Figure 5B) assemblies are commonly observed. In general, this structural feature can introduce additional connecting capacity for individual nanobuilding blocks. It is understandable that the tiny TiO_2 nanorods on the surface region would partially penetrate one another, essentially analogous to the "detachable adhesive tape" where an excellent adhesive effect is expected.[66] A similar interconnecting effect can also be observed in the flowerlike or rodlike ZnO phase on the $H_2Ti_5O_{11}\cdot H_2O$ (Figure 7), $TiO_2/H_2Ti_5O_{11}\cdot H_2O$ (Figure 10), and TiO_2 (Figure 11) bases, due to their surface "roughness". Combinations among these puffy nanocomposites can be further performed via simple physical mixing.

(ii) In addition to the enhancement in interconnectivity, the above surface feature will prevent the simple aggregation or coalescence of the primary phases (such as $H_2Ti_5O_{11}\cdot H_2O$, TiO_2, or ZnO) that takes place commonly for monocomponent nanomaterials, since the primary phases (which were first introduced) are clearly separated by the phases introduced later.

(66) Liu, B.; Zeng, H. C. *J. Am. Chem. Soc.* **2004**, *126*, 8124−8125.

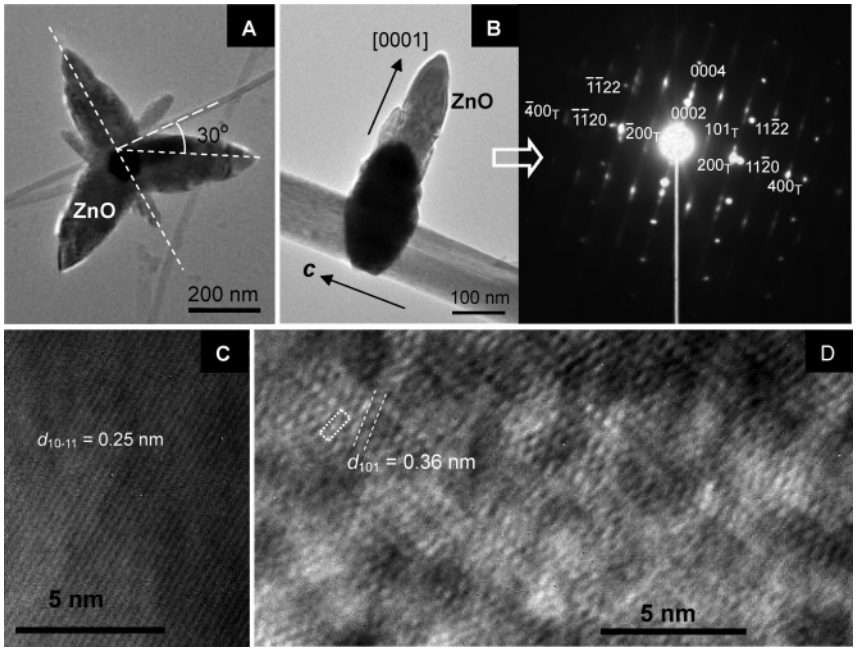

Figure 9. TEM analysis on as-prepared flowerlike $ZnO/H_2Ti_5O_{11}\cdot H_2O$ nanocomposite: (A) geometrical relationship between ZnO "flower" and $H_2Ti_5O_{11}\cdot H_2O$ nanobelt ("stem"), (B) an SAED pattern of $ZnO/H_2Ti_5O_{11}\cdot H_2O$ ([010] zone spots of anatase TiO_2 are indicated with a subscript "T", and the rest are [1−100] zone spots of wurtzite ZnO), (C) HRTEM image of ZnO lattice fringes, and (D) HRTEM image of a decomposing $H_2Ti_5O_{11}\cdot H_2O$ nanobelt where the {010} planes (the framed area indicates a surface unit cell of $a_o \times c_o$) of anatase TiO_2 can be observed.

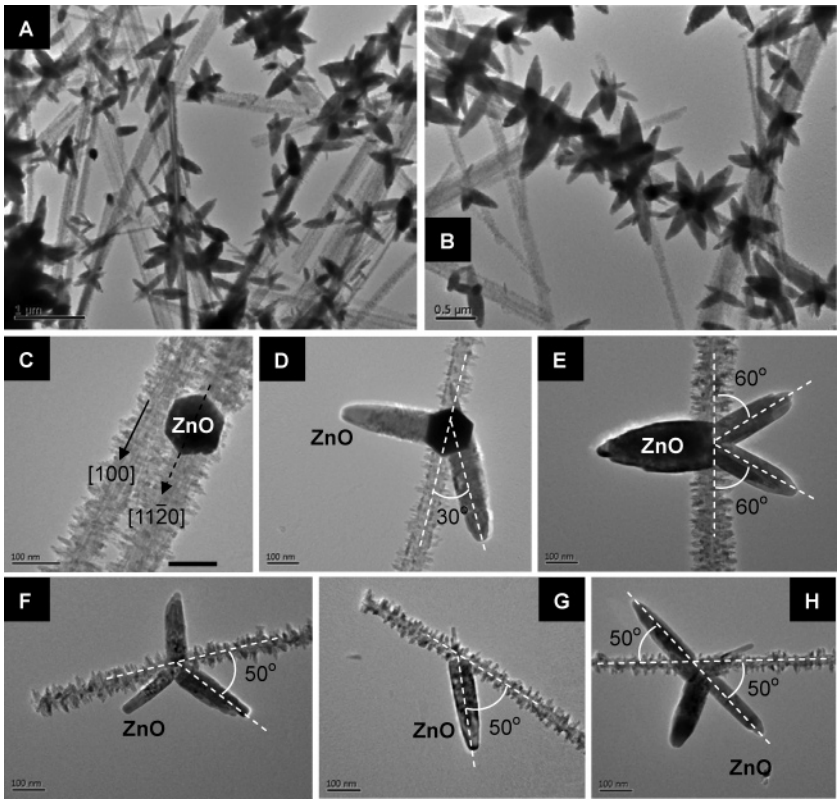

Figure 10. TEM images of the bamboolike $ZnO/TiO_2/H_2Ti_5O_{11}\cdot H_2O$ nanocomposite prepared by adding as-prepared $TiO_2/H_2Ti_5O_{11}\cdot H_2O$ nanobelts (Figure 5) into a 0.010 M $ZnSO_4$ aqueous solution containing ammonium fluoride (molar ratio $NH_4^+/Zn^{2+} = 30$, pH = 11.66) at 60 °C for 7 h.

For the single-phase nanomaterials, several growth mechanisms regarding agglomeration of primary particles have been well understood. For instance, "oriented attachments" of TiO_2 and ZnO nanoparticles have been observed respectively in recent years.[37,39,67] Nonetheless, this mechanism is unlikely responsible for the coalescence of the nanocomposites prepared in this work. Because of anchoring on the primary basis, it would be difficult for the surface nanostructures to adjust their positions to match correct crystallographic planes of the neighboring structures, especially for those with long nanobelts (Figures 7 and 10).

(67) Penn, R. L.; Banfield, J. F. *Science* **1998**, *281*, 969−971.

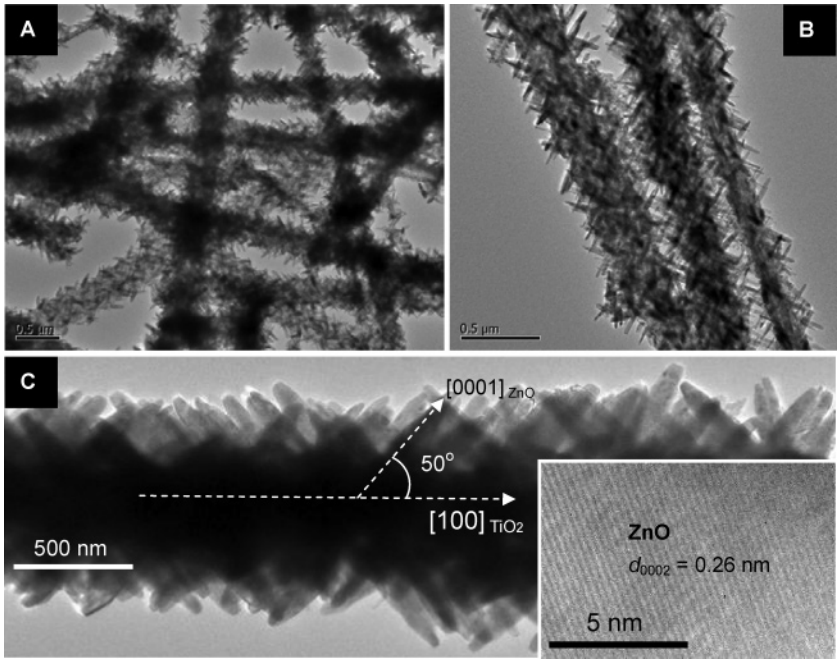

Figure 11. TEM images (A to C) of ZnO/TiO_2 nanocomposite prepared by adding as-prepared TiO_2 nanostructures (Figure 6) into a 0.010 M $ZnSO_4$ aqueous solution containing ammonium fluoride (molar ratio $NH_4^+/Zn^{2+} = 30$, pH = 11.66) at 60 °C for 7 h. Inset in part C shows an HRTEM image of ZnO nanorods.

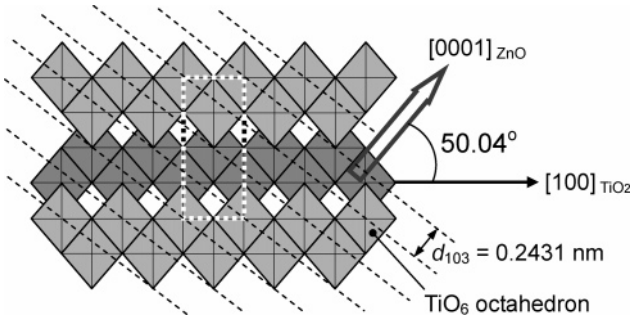

Figure 12. A schematic illustration of growth directions of ZnO nanorods on the {103} crystal planes of TiO_2 in the ZnO/TiO_2 nanocomposites. Dashed lines indicate the {103} crystal planes of TiO_2, and the dotted frame shows a unit cell of anatase TiO_2 viewed along the [010] direction.

Due to lack of space freedom, the direct crystal "fusion" of composite nanobuilding blocks is not observed.

(iii) The presence of extruding surface phases would simply imply that a lower specific weight or low density can be achieved for this type of puffy nanocomposite. In this regard, a higher density would be expected for those with shorter building blocks, while a lower density, for those with long and intricate structures, because a greater space constraint that hinders the agglomeration is anticipated in the latter case.

Conclusions

In summary, novel oxide nanocomposites of $TiO_2/H_2Ti_5O_{11}\cdot H_2O$, $ZnO/H_2Ti_5O_{11}\cdot H_2O$, $ZnO/TiO_2/H_2Ti_5O_{11}\cdot H_2O$, and ZnO/TiO_2 with high structural complexity can be prepared in aqueous solutions. When prepared into nanobelts, the protonated pentatitanate $H_2Ti_5O_{11}\cdot H_2O$ has been proved to be a suitable templating material for depositions of TiO_2 and/or ZnO, offering a high synthetic flexibility and a rich variety of morphological and structural tailoring. In binary nanocomposite $TiO_2/H_2Ti_5O_{11}\cdot H_2O$, for example, TiO_2 can be arranged into fishbonelike superstructures with their ⟨001⟩ axes perpendicular to the *c*-axis of the $H_2Ti_5O_{11}\cdot H_2O$ nanobelts. Furthermore, the encapsulated nanobelts can be removed with an additional hydrothermal treatment, giving away a new type of TiO_2 nanocrystal array with hollow interiors. Instead of the above deposition, discrete flowerlike ZnO multipods can be selectively grown onto the $H_2Ti_5O_{11}\cdot H_2O$ nanobelts with defined crystallographic orientations (i.e., [11−20] of ZnO is parallel to the *c*-axis of the nanobelts). In addition to this, the discrete ZnO multipods can also be deposited onto the as-prepared $TiO_2/H_2Ti_5O_{11}\cdot H_2O$, resulting in a tertiary nanocomposite $ZnO/TiO_2/H_2Ti_5O_{11}\cdot H_2O$. On the other hand, directional deposition of ZnO can be achieved when the nanostructured template of TiO_2 is used. In the latter nanocomposite, ZnO nanorods are grown and aligned evenly on the surfaces of one-dimensional TiO_2 nanocrystal arrays at a projecting angle of 50° with respect to the propagating direction of TiO_2 arrays (i.e., [100]). The extruding surface phases may generate a newer organization capacity among the puffy nanobuilding blocks, resulting in low-density nanomaterials. In addition to materials consideration, the art and science of organizing individual nanocomponents should deserve more research attention in future design and fabrication of nanocomposites.

Acknowledgment. The authors gratefully acknowledge research funding supported by the Ministry of Education, Singapore and the National University of Singapore.

Supporting Information Available: TEM, SAED, and HRTEM results (PDF). This material is available free of charge via the Internet at http://pubs.acs.org.

JA045253X